

Semiclassical Nonadiabatic Molecular Dynamics Using Linearized Pair-Density Functional Theory

Matthew R. Hennefarth,¹ Donald G. Truhlar,^{2,*} and Laura Gagliardi^{3,4,†}

¹*Department of Chemistry and Chicago Center for Theoretical Chemistry, University of Chicago, Chicago, IL 60637, USA*

²*Department of Chemistry, Chemical Theory Center, and Minnesota Supercomputing Institute, University of Minnesota, Minneapolis, MN 55455-0431, USA*

³*Department of Chemistry, Pritzker School of Molecular Engineering, The James Franck Institute, and Chicago Center for Theoretical Chemistry, University of Chicago, Chicago, IL 60637, USA*

⁴*Argonne National Laboratory, 9700 S. Cass Avenue, Lemont, IL 60439, USA*

(Dated: September 13, 2024)

Nonadiabatic molecular dynamics is an effective method for modeling nonradiative decay in electronically excited molecules. Its accuracy depends strongly on the quality of the potential energy surfaces, and its affordability for long direct-dynamic simulations with adequate ensemble averaging depends strongly on the cost of the required electronic structure calculations. Linearized pair-density functional theory (L-PDFT) is a recently developed post-self-consistent field multireference method that can model potential energy surfaces with an accuracy similar to expensive multireference perturbation theories but at a computational cost similar to the underlying multi-configuration self-consistent field method. Here we integrate the SHARC dynamics and PySCF electronic structure code to utilize L-PDFT for electronically nonadiabatic calculations and use the combined programs to study the photoisomerization reaction of *cis*-azomethane. We show that L-PDFT is able to successfully simulate the photoisomerization and yields results similar to the more expensive extended multi-state complete active space second-order perturbation theory. This shows that L-PDFT can model internal conversion, and it demonstrates its promise for broader photodynamics applications.

Nonadiabatic molecular dynamics is a valuable tool for modeling nonradiative decay pathways in molecules. The quality of the dynamics depends on the accuracy of the potential energy surfaces on which the nuclei move, but obtaining good accuracy for excited-state potential energy surfaces is difficult due to the inherently multiconfigurational nature of excited-state wave functions and the need for consistent treatment of close-lying states. State-averaged complete active space self-consistent field (SA-CASSCF)¹⁻³ is a widely used multireference method that generates qualitatively accurate and consistent wave functions for a set of orthogonal states, but it does not yield quantitatively accurate potential energy surfaces. Multi-state multireference perturbation methods such as multi-state complete active space second-order perturbation theory (MS-CASPT2)^{4,5} or quasidegenerate *n*-electron valence state second-order perturbation theory (QD-NEVPT2)^{6,7} use SA-CASSCF wave functions as a starting point to achieve better quantitative accuracy; however, they are computationally expensive. This limits their use to molecular dynamics of small molecular systems with small active spaces, short-timescale dynamics, or limited ensemble averaging.

Multiconfiguration pair-density functional theory (MC-PDFT)⁸⁻¹⁰ is an alternative post-SCF method that can yield accurate energies similar to complete active space second-order perturbation theory (CASPT2)¹¹ or *n*-electron valence state second-order perturbation the-

ory (NEVPT2)¹² but at a fraction of the computational cost. Additionally, MC-PDFT has been shown to agree with MS-CASPT2⁵ for intersystem crossing dynamics (population transfer to states of different spin symmetry) of thioformaldehyde, whereas SA-CASSCF overestimated the population transfer.¹³⁻¹⁵ MC-PDFT computes the total energy of a multiconfigurational wave function using a functional of the electron density and on-top pair density; however, it is a single-state method (it calculates the energy of each state independently of the other states). Single-state methods cannot accurately model the potential energy surfaces near regions of strong nuclear-electronic coupling such as at conical intersections, locally avoided crossings, or when many electronic states lie close in energy (as is common in actinides). As such, it is not an appropriate method for modeling internal conversion processes (population transfer to states of the same spin symmetry).

Linearized pair-density functional theory (L-PDFT)¹⁶ is a recently developed multi-state extension of MC-PDFT that can properly model potential energy surfaces near regions of strong nuclear-electronic coupling. L-PDFT defines an effective Hamiltonian operator that is a functional of the model-space averaged density and on-top pair density with the property that its eigenvalues are linear approximations to the MC-PDFT energies of the states. It is an example of a multi-state method in which diagonalization of the effective Hamiltonian operator within the model space yields potential energy surfaces with the correct topology near conical intersections and locally avoided crossings. L-PDFT has recently been shown to be as accurate as

* corresponding author: truhlar@umn.edu

† corresponding author: lgagliardi@uchicago.edu

MC-PDFT and NEVPT2 at predicting vertical excitation energies for over 400 excitations in the QUESTDB database,¹⁷ it is slightly faster than MC-PDFT, it does not suffer from the intruder-state problem,¹⁸ it does not require the iterative solution of a large set of linear perturbation-theory equations,⁵ and it does not require iterative steps to find an intermediate basis to construct an effective model-space Hamiltonian.¹⁹ All of these attributes make L-PDFT a very promising method for modeling excited-state dynamics. Recent development of L-PDFT analytic nuclear gradients²⁰ as well as curvature-driven approximations to the time-derivative coupling for dynamics calculations^{21–24} allows one to use L-PDFT for modeling internal conversion processes using semiclassical nonadiabatic molecular dynamics methods such as curvature-driven trajectory surface hopping (κ TSH)^{22,25,26} or curvature-driven coherent switching with decay of mixing (κ CSDM).^{27–29}

Here we implement a SHARC-PySCF interface that allows the SHARC^{30,31} dynamics program to use the PySCF^{32,33} electronic structure program for L-PDFT κ TSH direct-dynamics calculations of the *cis-to-trans* photoisomerization reaction of azomethane (fig. 1). One reason to choose this reaction for our initial study is that it has been widely studied both experimentally and theoretically.^{34–40} A second reason is the very informative recent study of this system by several methods³⁵ that quantified how single-reference methods such as second-order algebraic diagrammatic construction (ADC(2)),⁴¹ second-order coupled cluster (CC2),⁴² configuration interaction singles (CIS),^{43,44} and time-dependent density functional theory (TD-DFT)^{45,46} are unable to satisfactorily simulate the *cis-to-trans* isomerization because the majority of the trajectories crash and that also found a large number of crashes when using multireference methods. Troublesome trajectories are a bane of this field because one must obtain continuous and smooth convergence of iterative calculations over the wide nuclear configuration space explored in typical photodissociation reactions. We study this problem in detail and show below that L-PDFT is a robust method for this system, for which it yields results similar to extended multistate complete active space second-order perturbation theory (XMS-CASPT2),⁴⁷ while keeping the computational cost only slightly larger than that of the reference SA-CASSCF method.

All electronic structure calculations reported here, except XMS-CASPT2 and frequency calculations, were performed with PySCF^{32,33} (Version 2.5.0, commit v1.1-8184-geaefc35752) compiled with LIBCINT⁴⁸ (Version 6.1.1) and LIBXC^{49,50} (Version 6.1.0) and used the `csf_solver` from MRH.⁵¹ Additionally, all L-PDFT calculations used PySCF-FORGE⁵² (commit SHA-1 f817911), an extension module for PySCF. All geometry optimizations used the GEOMETRIC package⁵³ (Version 1.0) in PySCF. All PDFT calculations used the tPBE on-top functional.^{8,54} (All XMS-CASPT2 and SA-CASSCF frequency calculations were

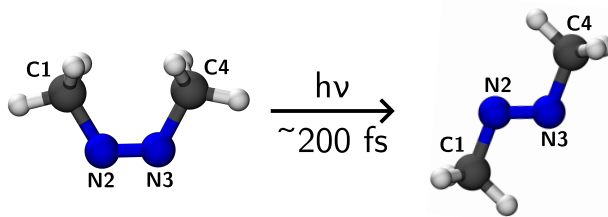


FIG. 1. The *cis-to-trans* photoisomerization of azomethane. blue: nitrogen, grey: carbon, white: hydrogen.

performed in OPENMOLCAS⁵⁵ (Version 24.02, commit v24.02-127-gd603295fc). The XMS-CASPT2 calculations were performed with no ionization-potential–electron-affinity (IPEA) shift,⁵⁶ with an imaginary level shift⁵⁷ of 0.3i, and density fitting.⁵⁸ All software used here is free and open-source available to the whole community.

No spatial symmetry was enforced in any calculation. All calculations of azomethane used the 6-31G* basis set⁵⁹ and state averaging over the lowest two singlet states (S_0 and S_1). We used a quadrature grid size of 4 (60/90 radial points and 434/590 angular points for atoms of periods 1 and 2 respectively). The L-PDFT vertical excitation energies using grids 4 and 6 do not change (at least to the hundredths place). This agrees with our prior studies which showed that a level-3 grid is sufficient.^{12,17}

We first investigate the suitability of L-PDFT for describing the vertical excitation energy of the first excited singlet state of *cis-* and *trans-*azomethane, which is an $n \rightarrow \pi^*$ excitation. Table 1 summarizes the vertical excitation energies calculated using SA-CASSCF, L-PDFT, and XMS-CASPT2; and, it also includes results from resolution-of-the-identity second-order algebraic diagrammatic construction (RI-ADC(2)), multireference configuration interaction (MRCI),⁶⁰ multireference configuration interaction singles and doubles with Davidson size-extensivity correction (MRCISD+Q),^{61,62} and third-order coupled cluster (CC3).^{42,63} The SA-CASSCF, L-PDFT, and XMS-CASPT2 vertical excitation energies were calculated at their equilibrium geometries optimized with their respective methods. Table 1 also includes experimental degassed aqueous⁶⁴ and gas phase⁶⁵ *trans*-isomer vertical excitation energies. The table shows that our results with two different active spaces agree well with the experimental results,^{64,65} as do the XMS-CASPT2 and RI-ADC(2) calculations, and we find that the L-PDFT calculations are more accurate than the SA-CASSCF, MRCI, and MRCISD+Q calculations. The good accuracy is consistent with our previous tests of L-PDFT.^{16,17}

Next we performed nonadiabatic molecular dynamics simulations. All dynamics simulations were performed using a locally modified version of SHARC^{30,31} (version 3.0, commit SHA-1 afefdb8) using κ TSH with energy-

TABLE 1. Vertical excitation energies (in eV) of the first excited singlet state of azomethane at the *cis* or *trans* geometries.

Method	Basis	Active Space ^a	<i>cis</i>	<i>trans</i>
SA-CASSCF	6-31G*	(6e,4o)	3.63	3.80
SA-CASSCF	6-31G*	(10e,8o)	3.85	3.99
L-PDFT	6-31G*	(6e,4o)	3.30	3.55
L-PDFT	6-31G*	(10e,8o)	3.31	3.52
XMS-CASPT2	6-31G*	(6e,4o)	3.38	3.60
XMS-CASPT2	6-31G*	(10e,8o)	3.47	3.68
RI-ADC(2) ³⁷	aug-cc-pVTZ		3.50	3.66
MRCI ³⁷	6-31G*	(6e,4o)	3.62	3.82
MRCISD+Q ^{b66}	cc-pVTZ			3.77
CC3 ^{c67}	aug-cc-pVDZ			3.76
expt. (aqueous) ⁶⁴				3.60
expt. (gas phase) ⁶⁵				3.65

^a The notation (*me, no*) denotes *m* active electrons in *n* active orbitals. The (6e,4o) active space is composed of the π and π^* orbitals and the two nitrogen lone-pair orbitals.

^b Calculated at MP2/6-311G(2d,2p) optimized geometry. Reference orbitals are from SA-CASSCF(6e,4o) calculation.

^c Calculated at CCSD/cc-pVDZ optimized geometry.

based decoherence. Specifically, we used the fewest switches algorithm²⁵ with the curvature-driven approximation to the time-derivative coupling (calculated with the gradient formula²²) with the energy-based decoherence scheme.²⁶ The curvature-driven approximation has been shown to perform similarly to calculating the full nonadiabatic coupling vector for this photoisomerization reaction.⁴⁰ An advantage of curvature-driven dynamics methods is that they do not require nonadiabatic coupling matrix elements or wave function overlaps between states with different geometries. A new interface script was added to allow PySCF to be used as the direct-dynamics electronic structure solver. Initial conditions (geometries and velocities) were generated in SHARC using a Wigner distribution without temperature broadening. L-PDFT and SA-CASSCF trajectories were run with the same initial conditions where the harmonic frequencies used in the Wigner distribution were computed for the SA-CASSCF ground state in OPENMOLCAS. We used a fixed nuclear time step of 0.5 fs, and the electronic wave function was propagated using a 0.0025 fs time step. The decoherence parameter of the energy-based decoherence was set to 0.1 hartrees. The velocity vector was not modified when a frustrated hop was encountered. To conserve energy during a hop, the total velocity vector was rescaled, which is not likely to strongly impact the final dynamics.⁶⁸ We performed dynamics calculations starting in the S_1 state of the *cis* isomer and propagated each trajectory for 150 fs

We first used the smaller (6e,4o) active space (fig. S1). We confirmed good energy conservation for each trajectory by verifying that the total energy variation was less than 0.2 eV for the entire trajectory and less than 0.1 eV between each step. We ran 150 trajectories with

TABLE 2. Number of trajectories at each level of theory that did not conserve energy within 0.2 eV.

Method	(6e,4o)	(10e,4o)
SA-CASSCF	1	3
L-PDFT	5	7

SA-CASSCF and 150 with L-PDFT, and only one SA-CASSCF trajectory and five L-PDFT trajectories failed to meet these energy conservation criteria (table 2). The single problematic SA-CASSCF trajectory very quickly failed to conserve energy (fig. S5) and also quickly failed for L-PDFT (fig. S6); therefore we omit this trajectory from all further discussion because it is likely due to a bad initial condition.

The L-PDFT failure rate corresponds to only 3%, which compares favorably to a prior study of failure rates using XMS-CASPT2 with the same active space that reported over 10% of the trajectories crashing within 150 fs³⁵ (although it was unstated which part of the calculations failed or if they could be restarted). We conclude that L-PDFT κ TSH trajectories are less troublesome than trajectories with XMS-CASPT2 and that L-PDFT is well-suited for dynamics simulations.

In order to better understand the cause of trajectory failure, we inspected the L-PDFT trajectories that did not conserve energy. We found that energy-conservation failure occurred after relaxation to the S_0 state and when one of the C–N bonds is breaking. Figure 2 shows the C–N bond lengths as functions of time as well as the absolute bond-length difference (aBLD) for both the SA-CASSCF and L-PDFT trajectories. Trajectories are colored in red after the point at which they no longer conserve energy. SA-CASSCF with the (6e,4o) active space does not have any trajectories for which the C–N breaks, which is consistent with prior simulations using this active space.^{37,38} On the other hand, for each of the (6e,4o) L-PDFT trajectories that does not conserve energy, the bond has already broken or is breaking. Since the (6e,4o) active space does not include any C–N bonding or antibonding orbitals, it is likely that orbitals are rotating into and out of the active space in order to describe the bond breaking. This kind of behavior can cause discontinuous derivatives of the SA-CASSCF potential energy surface, and it causes discontinuous potential energy surfaces for post-SA-CASSCF methods such as L-PDFT and XMS-CASPT2. The lack of non-energy-conserving trajectories in the SA-CASSCF calculations is because SA-CASSCF never explores the dissociation region of the potential energy surface.

To confirm the above interpretation of the problematic trajectories, we performed rigid scans of the energy along the C1-N2 bond-breaking coordinate starting from the L-PDFT optimized *cis*- and *trans*-isomer structures. Figure 3 shows the potential energy curves for the S_0 and S_1 states computed by SA-CASSCF, XMS-CASPT2, and L-PDFT. Starting with the orbitals in fig. S1, the *cis*

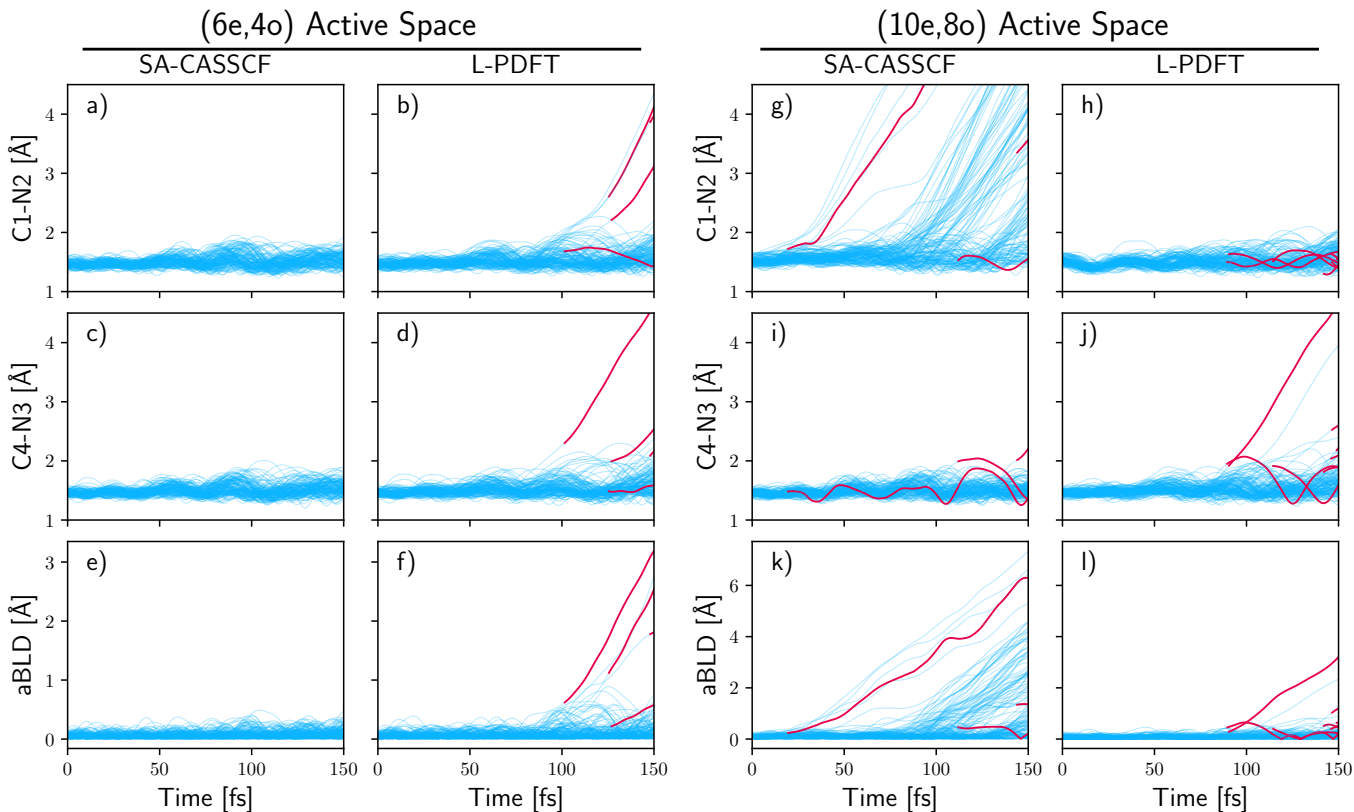


FIG. 2. Time evolution of the C1-N2 and C4-N3 bonds as well as the absolute bond-length difference (aBLD) between these two bonds for both the (6e,4o) and (10e,8o) active space. Blue curves represent trajectories that terminated normally and red curves represent portions of trajectories that no longer conserved total energy.

scan proceeds smoothly until about 3.4 \AA at which point the solutions disappear. Scanning in the reverse direction shows a different solution, which can be followed until about 2.2 \AA , with the energy of this solution crossing that of the forward scan solution. At the crossing point, the minimum-energy SA-CASSCF solution must switch with a discontinuous derivative, and the crossing causes discontinuous curves for L-PDFT and XMS-CASPT2. This is unsurprising because the (6e,4o) active space is not appropriate for describing the C–N photodissociation process. Panels a and c of fig. 3 show that the SA-CASSCF potential energy curves require a relatively large amount of energy for C–N dissociation, even before the cross-over point (in particular about 4 eV and 5 eV on the ground state for the *cis* and *trans* isomers respectively in agreement with prior theoretical studies.³⁸ L-PDFT agrees more closely with XMS-CASPT2 which has a substantially lower energy requirement for C–N dissociation before the cross-over point, about 2 eV.

Experimentally and theoretically, it is known that C–N bond dissociation (after relaxation to the electronic ground state) is a possible photoproduct for azomethane.³⁸ Prior simulations using XMS-CASPT2 with the same (6e,4o) active space³⁸ and MRCI,³⁷ and experiments^{69,70} of *cis*- and *trans*-azomethane photoisomerization also had several C–N bonds dissociating

within 150 fs, although the computational studies did not specify how well any of these trajectories conserved total energy. Given the inability of the smaller (6e,4o) active space to properly describe this bond dissociation, it is likely that a significant number of XMS-CASPT2 trajectories in the prior study did not conserve energy after one of the C–N bonds broke. Evidently, the failure of a few L-PDFT trajectories to conserve energy with the (6e,4o) active space is due to the inability of this small active space to properly describe the C–N dissociation, rather than being an issue with the L-PDFT method.

To model the C–N bond dissociation pathway, we carried out dynamics calculations using the larger (10e,8o) active space that includes the C1-N2 bonding and antibonding orbitals (fig. S3 and S4). The (10e,8o) active space also includes N–N σ and σ^* orbitals. Although our initial active space is not symmetric, the molecular geometry during the course of the simulation will rarely (if ever) have any point group symmetry. Using the larger active space, all of the trajectories finished, and only three SA-CASSCF and seven L-PDFT trajectories of the 150 total trajectories (less than 5%) failed to conserve total energy (table 2). Again this compares favorably to the previous XMS-CASPT2 study, which had over 10% crashed trajectories. Inspection of the C–N bonds in the new batch of trajectories shows that SA-

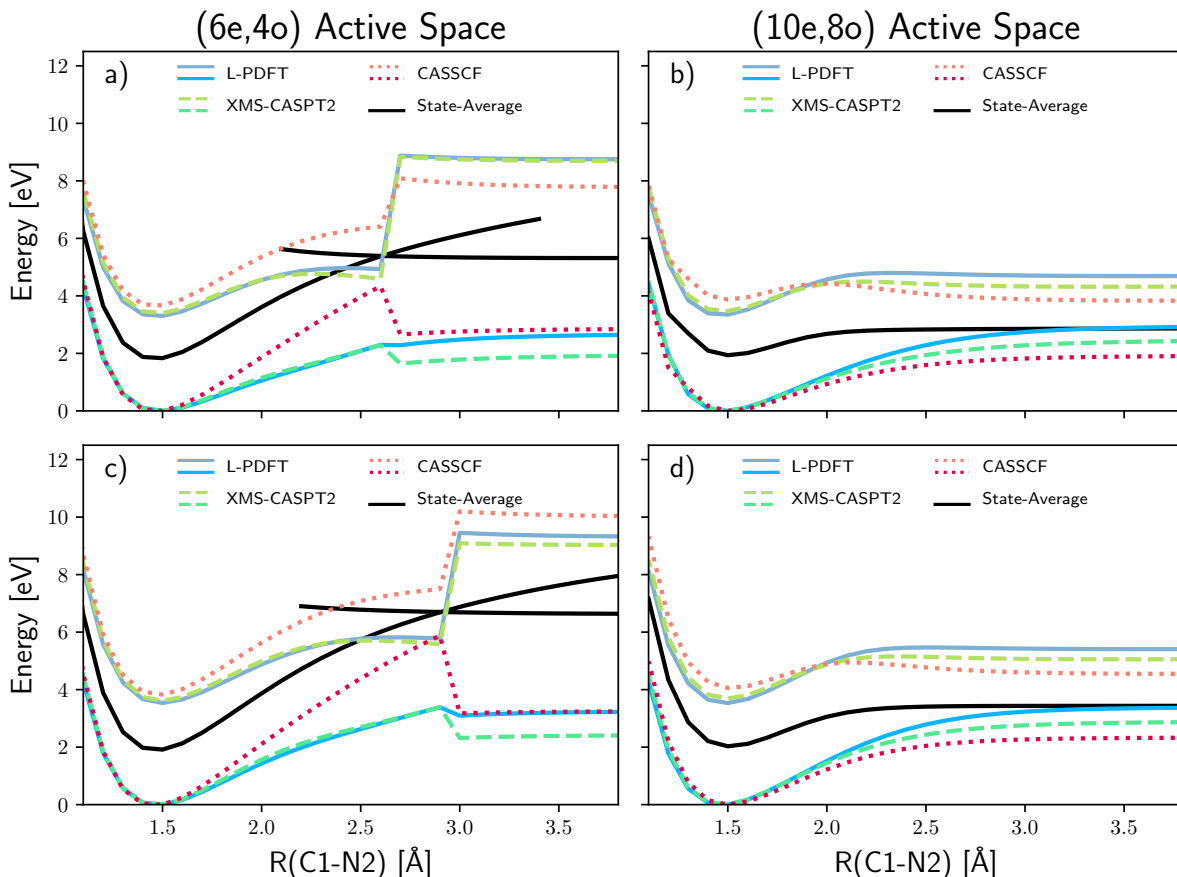


FIG. 3. Potential energy scans of the lowest two singlet states of azomethane as computed with XMS-CASPT2, L-PDFT, and SA-CASSCF for two directions of scanning ((a,b) starting with *cis*; (c,d) starting with *trans*), each with with two different active spaces ((a,c) using (6e,4o); (b,d) using (10e,8o)). Starting structures are from the L-PDFT optimized structures at each respective isomer. Black curves represent the state-averaged SA-CASSCF energy.

CASSCF now has many trajectories with C1-N2 bond breaking and no trajectories with C4-N3 bond breaking. This is rationalized from the rigid potential energy curves in panels b and d of fig. 3 where SA-CASSCF with the (10e,8o) active space predicts a lower energy for C–N dissociation as compared to the smaller (6e,4o) active space. However, since there are no C4-N3 bonding/antibonding orbitals in the active space, it is likely that there needs to be a significant excess of energy, similar to that seen in the (6e,4o) active space, to dissociate the C4-N3 bond. Further, the number of trajectories exhibiting C–N bond dissociation, and the fast speed at which dissociation occurs (bonds breaking almost immediately), are unphysical. A prior study of SA-CASSCF dynamics using *ab initio* multiple spawning and a similar (10e,8o) active space also had a significant number of trajectories with C–N bond dissociation.³⁶ However, experimental evidence suggests that the photodissociation is a minor product and that bond dissociation does not occur on the excited state and should occur only after the molecule has reached the ground state (no trajectories reach the ground state until after 30 fs as shown in

fig. 4).^{69–72} L-PDFT no longer has any C1-N2 bond dissociations, and instead only the C4-N3 bonds are breaking (fig. 3). This is likely due to the active space not containing the C4-N3 bonding or antibonding orbitals giving results similar to the (6e,4o) active space. When energy nonconservation occurs with the larger active space, it is likely due to the inadequacy of this active space to properly model the C4-N3 bond breaking. An even larger active space would be required in order to properly model both C–N bond dissociations; although this is computationally feasible for this small system, it is beyond the scope of the current letter.

Using only those trajectories that conserved energy and terminated normally, fig. 4 shows the time-dependent electronic state populations and isomer percentage for each method and active space. Both SA-CASSCF and L-PDFT have an induction period of about 30 fs and then rapidly decay from S_1 to S_0 until about 60 fs. During this time, almost all trajectories have switched to the *trans* isomer. A second plateau in the electronic populations then lasts for about 45 fs at which point the molecule reaches a second strong-coupling region as some

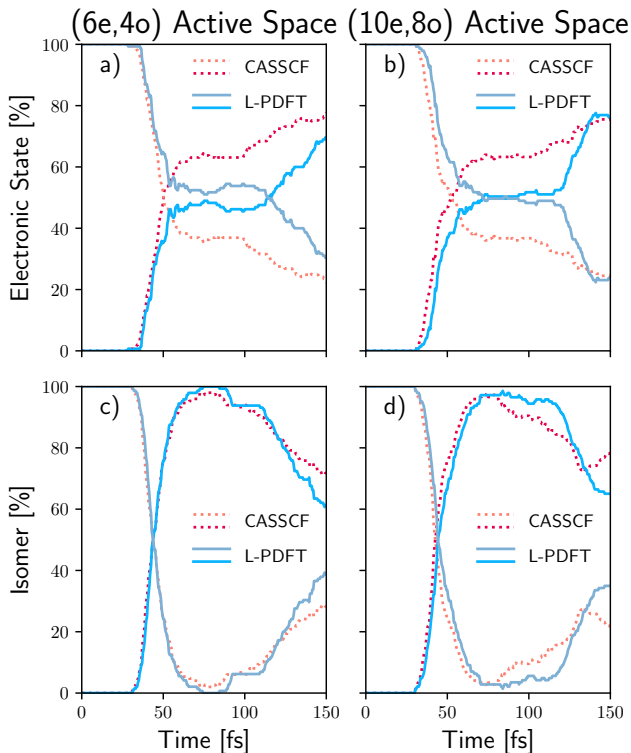


FIG. 4. Ensemble-averaged electronic state population (a,b) and isomer percentages (c,d) as functions of time using the smaller (6e,4o) (a,c) and larger (10e,8o) (b,d) active spaces. All trajectories were started in the S₁ state of the *cis* isomer.

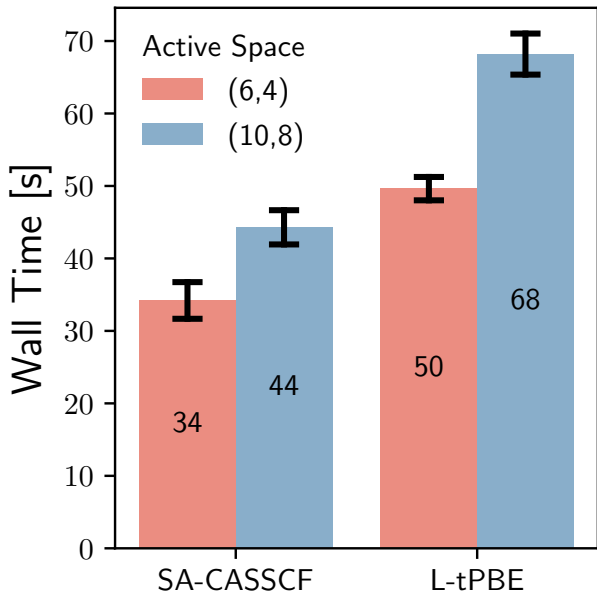


FIG. 5. Average wall time for each step of the dynamics. Only normal terminating trajectories are considered. Black bars represent standard deviation.

molecules go from *trans* to *cis* isomers. The primary difference between the two methods is the speed at which the molecules relax to the ground state. SA-CASSCF predicts faster decay with over 60 % of the trajectories relaxing to the S₀ state after passing the first region of strong-coupling whereas L-PDFT predicts about 45 %. Prior studies have similarly noted that SA-CASSCF overestimates the short-time decay rate as compared to both XMS-CASPT2 and MS-CASPT2.^{35,38–40}

Figure 4 of the present study may be directly compared to fig. 1 of Papineau et al.³⁵. This shows that the present L-PDFT ensemble-averaged populations and isomer percentages, for both active spaces, agree well the prior MS-CASPT2 results. This shows that L-PDFT is a robust method that can yield results as accurate as the more expensive MS-CASPT2 and XMS-CASPT2 method.

We also confirm that the L-PDFT simulations may be carried out efficiently. Figure 5 summarizes the average wall time for each step of the dynamics for both SA-CASSCF and L-PDFT with both active spaces. All calculations were performed using 2 cores with 8 GB of memory on an Intel Xeon Gold 6248R processor. Each step involves a single-point calculation as well as two gradient calculations: one for each state. The gradient calculations were done in parallel, with each using a single core. The wall time for each step represents the time for the single-point calculation and the maximum time needed to perform either of the gradient calculations plus any other time needed by the SHARC driver (which corresponds to “overhead” and should be minimal). For both active spaces, L-PDFT steps take on average only 1.5 times as long as SA-CASSCF.

Our implementation so far is not fully optimized. For example, caching intermediate quantities within the SHARC-PySCF interface could speed up gradient calculations, and implementation of density fitting⁷³ could also be used to speed up future calculations.

In this letter, we have presented the implementation of an interface between SHARC and PySCF in order to leverage the accuracy and computational efficiency of L-PDFT for nonadiabatic molecular dynamics. To demonstrate the capability of the method, we have studied the *cis*-to-*trans* photoisomerization of azomethane. Utilizing both a smaller and a larger active space, no L-PDFT trajectories crashed, which compares favorably with prior studies utilizing XMS-CASPT2 for the same system where more than 10 % of the trajectories crashed.³⁵ Like XMS-CASPT2, L-PDFT highlights the importance of the C–N photodissociation product. We found that only a small fraction of the trajectories did not conserve energy (table 2), and we showed that the few failures found were due to the active space not properly modeling C–N dissociation. We showed that L-PDFT adds only a small computational cost over SA-CASSCF (fig. 5), and it provides a slower population decay more similar to MS-CASPT2.³⁵ In summary, we find that L-PDFT is a promising new multireference method that is able to provide results similar to the much more

expensive multireference perturbation theories at a computational cost only slightly more expensive than SA-CASSCF. We also found that L-PDFT is more robust than traditional multireference perturbation theories for molecular dynamics.

SUPPORTING INFORMATION

Active spaces used, total energy deviation as a function of time, geometrical distributions at surface hops, optimized azomethane coordinates, harmonic frequencies used in the Wigner distribution, and example input files for SHARC.

ACKNOWLEDGMENTS

This work was supported in part by the Air Force Office Scientific Research (grant no. FA9550-20-1-0360). M.R.H. acknowledges support by the National Science Foundation Graduate Research Fellowship Program (grant no. 2140001). Any opinions, findings, and conclusions or recommendations expressed in this material are those of the author(s) and do not necessarily reflect the views of the National Science Foundation. We also acknowledge the University of Chicago's Research Computing Center for their support of this work.

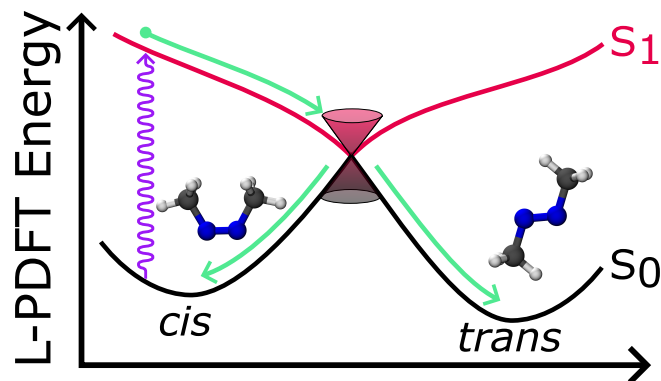
REFERENCES

- [1] Roos, B. O.; Taylor, P. R.; Sigbahn, P. E. M. A complete active space SCF method (CASSCF) using a density matrix formulated super-CI approach. *Chem. Phys.* **1980**, *48*, 157–173.
- [2] Ruedenberg, K.; Cheung, L. M.; Elbert, S. T. MCSCF optimization through combined use of natural orbitals and the brillouin-levy-berthier theorem. *Int. J. Quantum Chem.* **1979**, *16*, 1069–1101.
- [3] Roos, B. O. The complete active space self-consistent field method and its applications in electronic structure calculations. *Adv. Chem. Phys.* **1987**, *69*, 399–445.
- [4] Andersson, K.; Malmqvist, P. Å.; Roos, B. O.; Sadlej, A. J.; Wolinski, K. Second-order perturbation theory with a CASSCF reference function. *J. Phys. Chem.* **1990**, *94*, 5483–5488.
- [5] Finley, J.; Malmqvist, P.-Å.; Roos, B. O.; Serrano-Andrés, L. The multi-state CASPT2 method. *Chem. Phys. Lett.* **1998**, *288*, 299–306.
- [6] Angeli, C.; Cimraglia, R.; Evangelisti, S.; Leininger, T.; Malrieu, J.-P. Introduction of n -electron valence states for multireference perturbation theory. *J. Chem. Phys.* **2001**, *114*, 10252–10264.
- [7] Angeli, C.; Borini, S.; Cestari, M.; Cimraglia, R. A quasidegenerate formulation of the second order n -electron valence state perturbation theory approach. *J. Chem. Phys.* **2004**, *121*, 4043–4049.
- [8] Li Manni, G.; Carlson, R. K.; Luo, S.; Ma, D.; Olsen, J.; Truhlar, D. G.; Gagliardi, L. Multiconfiguration pair-density functional theory. *J. Chem. Theory Comput.* **2014**, *10*, 3669–3680.
- [9] Ghosh, S.; Verma, P.; Cramer, C. J.; Gagliardi, L.; Truhlar, D. G. Combining wave function methods with density functional theory for excited states. *Chem. Rev.* **2018**, *118*, 7249–7292.
- [10] Zhou, C.; Hermes, M. R.; Wu, D.; Bao, J. J.; Pandharkar, R.; King, D. S.; Zhang, D.; Scott, T. R.; Lykhin, A. O.; Gagliardi, L.; Truhlar, D. G. Electronic structure of strongly correlated systems: recent developments in multiconfiguration pair-density functional theory and multiconfiguration nonclassical-energy functional theory. *Chem. Sci.* **2022**, *13*, 7685–7706.
- [11] Hoyer, C. E.; Ghosh, S.; Truhlar, D. G.; Gagliardi, L. Multiconfiguration pair-density functional theory is as accurate as CASPT2 for electronic excitation. *J. Phys. Chem. Lett.* **2016**, *7*, 586–591.
- [12] King, D. S.; Hermes, M. R.; Truhlar, D. G.; Gagliardi, L. Large-scale benchmarking of multireference vertical-excitation calculations via automated active-space selection. *J. Chem. Theory Comput.* **2022**, *18*, 6065–6076.
- [13] Mai, S.; Atkins, A. J.; Plasser, F.; González, L. The influence of the electronic structure method on intersystem crossing dynamics. The case of thioformaldehyde. *J. Chem. Theory Comput.* **2019**, *15*, 3470–3480.
- [14] Zhang, L.; Shu, Y.; Sun, S.; Truhlar, D. G. Direct coherent switching with decay of mixing for intersystem crossing dynamics of thioformaldehyde: the effect of decoherence. *J. Chem. Phys.* **2021**, *154*, 094310.
- [15] Calio, P. B.; Truhlar, D. G.; Gagliardi, L. Nonadiabatic molecular dynamics by multiconfiguration pair-density functional theory. *J. Chem. Theory Comput.* **2022**, *18*, 614–622.
- [16] Hennefarth, M. R.; Hermes, M. R.; Truhlar, D. G.; Gagliardi, L. Linearized pair-density functional theory. *J. Chem. Theory Comput.* **2023**, *19*, 3172–3183.
- [17] Hennefarth, M. R.; King, D. S.; Gagliardi, L. Linearized pair-density functional theory for vertical excitation energies. *J. Chem. Theory Comput.* **2023**, *19*, 7983–7988.
- [18] Iijima, N.; Saika, A. A note on the convergence of multiconfigurational many-body perturbation theory. *Int. J. Quantum Chem.* **1985**, *27*, 481–493.
- [19] Bao, J. J.; Zhou, C.; Truhlar, D. G. Compressed-state multistate pair-density functional theory. *J. Chem. Theory Comput.* **2020**, *16*, 7444–7452.
- [20] Hennefarth, M. R.; Hermes, M. R.; Truhlar, D. G.; Gagliardi, L. Analytic nuclear gradients for complete active space linearized pair-density functional theory. *J. Chem. Theory Comput.* **2024**, *20*, 3637–3658.
- [21] Baeck, K. K.; An, H. Practical approximation of the non-adiabatic coupling terms for same-symmetry interstate crossings by using adiabatic potential energies only. *J. Chem. Phys.* **2017**, *146*, 064107.
- [22] Shu, Y.; Zhang, L.; Chen, X.; Sun, S.; Huang, Y.; Truhlar, D. G. Nonadiabatic dynamics algorithms with only potential energies and gradients: curvature-driven coherent switching with decay of mixing and curvature-driven trajectory surface hopping. *J. Chem. Theory Comput.* **2022**, *18*, 1320–1328.
- [23] do Casal, M. T.; Toldo, J. M.; Pinheiro Jr., M.; Barbatti, M. Fewest switches surface hopping with Baeck-An couplings. *Open Research Europe* **2022**, *1*.
- [24] Shu, Y.; Truhlar, D. G. Generalized Semiclassical Ehrenfest Method: A Route to Wave Function-Free Photo-

- chemistry and Nonadiabatic Dynamics with Only Potential Energies and Gradients. *J. Chem. Theory Comput.* **2024**, *20*, 4396–4426.
- [25] Tully, J. C. Molecular dynamics with electronic transitions. *J. Chem. Phys.* **1990**, *93*, 1061–1071.
- [26] Granucci, G.; Persico, M.; Zocante, A. Including quantum decoherence in surface hopping. *J. Chem. Phys.* **2010**, *133*, 134111.
- [27] Zhu, C.; Nangia, S.; Jasper, A. W.; Truhlar, D. G. Coherent switching with decay of mixing: an improved treatment of electronic coherence for non-Born–Oppenheimer trajectories. *J. Chem. Phys.* **2004**, *121*, 7658–7670.
- [28] Jasper, A. W.; Nangia, S.; Zhu, C.; Truhlar, D. G. Non-Born–Oppenheimer Molecular Dynamics. *Accounts Chem. Res.* **2006**, *39*, 101–108.
- [29] Shu, Y.; Zhang, L.; Mai, S.; Sun, S.; González, L.; Truhlar, D. G. Implementation of coherent switching with decay of mixing into the SHARC program. *J. Chem. Theory Comput.* **2020**, *16*, 3464–3475.
- [30] Mai, S.; Marquetand, P.; González, L. Nonadiabatic dynamics: the SHARC approach. *WIREs Comput. Mol. Sci.* **2018**, *8*, e1370.
- [31] Mai, S.; Avagliano, D.; Heindl, M.; Marquetand, P.; Menger, M. F. S. J.; Oettel, M.; Plasser, F.; Polonius, S.; Ruckebauer, M.; Shu, Y.; Truhlar, D. G.; Zhang, L.; Zobel, P.; González, L. SHARC3.0: surface hopping including arbitrary couplings – program package for non-adiabatic dynamics. 2023; <https://zenodo.org/records/7828641>.
- [32] Sun, Q.; Berkelbach, T. C.; Blunt, N. S.; Booth, G. H.; Guo, S.; Li, Z.; Liu, J.; McClain, J. D.; Sayfutyarova, E. R.; Sharma, S.; Wouters, S.; Chan, G. K. PySCF: the Python-based simulations of chemistry framework. *WIREs Comput. Mol. Sci.* **2017**, *8*, e1340.
- [33] Sun, Q. et al. Recent developments in the PySCF program package. *J. Chem. Phys.* **2020**, *153*, 024109.
- [34] Minezawa, N.; Nakajima, T. Trajectory surface hopping molecular dynamics simulation by spin-flip time-dependent density functional theory. *J. Chem. Phys.* **2019**, *150*, 204120.
- [35] Papineau, T. V.; Jacquemin, D.; Vacher, M. Which electronic structure method to choose in trajectory surface hopping dynamics simulations? Azomethane as a case study. *J. Phys. Chem. Lett.* **2024**, *15*, 636–643.
- [36] Ghosh, J.; Bhaumik, S.; Bhattacharya, A. Comparison of internal conversion dynamics of azo and azoxy energetic moieties through the (S1/S0)CI conical Intersection: An ab initio multiple spawning study. *Chem. Phys.* **2018**, *513*, 221–229.
- [37] Sellner, B.; Ruckebauer, M.; Stambolić, I.; Barbatti, M.; Aquino, A. J. A.; Lischka, H. Photodynamics of azomethane: a nonadiabatic surface-hopping study. *J. Phys. Chem. A* **2010**, *114*, 8778–8785.
- [38] Xu, C.; Lin, K.; Hu, D.; Gu, F. L.; Gelin, M. F.; Lan, Z. Ultrafast Internal Conversion Dynamics through the on-the-Fly Simulation of Transient Absorption Pump–Probe Spectra with Different Electronic Structure Methods. *J. Phys. Chem. Lett.* **2022**, *13*, 661–668.
- [39] Merritt, I. C. D.; Jacquemin, D.; Vacher, M. Nonadiabatic Coupling in Trajectory Surface Hopping: How Approximations Impact Excited-State Reaction Dynamics. *J. Chem. Theory Comput.* **2023**, *19*, 1827–1842.
- [40] Zhao, X.; Merritt, I. C. D.; Lei, R.; Shu, Y.; Jacquemin, D.; Zhang, L.; Xu, X.; Vacher, M.; Truhlar, D. G. Nonadiabatic coupling in trajectory surface hopping: accurate time derivative couplings by the curvature-driven approximation. *J. Chem. Theory Comput.* **2023**, *19*, 6577–6588.
- [41] Dreuw, A.; Wormit, M. The algebraic diagrammatic construction scheme for the polarization propagator for the calculation of excited states. *WIREs Comput. Mol. Sci.* **2015**, *5*, 82–95.
- [42] Christiansen, O.; Koch, H.; Jørgensen, P. The second-order approximate coupled cluster singles and doubles model CC2. *Chem. Phys. Lett.* **1995**, *243*, 409–418.
- [43] Bene, J. E. D.; Ditchfield, R.; Pople, J. A. Self-Consistent Molecular Orbital Methods. X. Molecular Orbital Studies of Excited States with Minimal and Extended Basis Sets. *J. Chem. Phys.* **1971**, *55*, 2236–2241.
- [44] Foresman, J. B.; Head-Gordon, M.; Pople, J. A.; Frisch, M. J. Toward a systematic molecular orbital theory for excited states. *J. Phys. Chem.* **1992**, *96*, 135–149.
- [45] Casida, M. E. *Recent Advances in Density Functional Methods*; Recent Advances in Computational Chemistry; World Scientific, 1995; Vol. Volume 1; pp 155–192.
- [46] Runge, E.; Gross, E. K. U. Density-Functional Theory for Time-Dependent Systems. *Phys. Rev. Lett.* **1984**, *52*, 997–1000.
- [47] Granovsky, A. A. Extended multi-configuration quasidegenerate perturbation theory: the new approach to multi-state multi-reference perturbation theory. *J. Chem. Phys.* **2011**, *134*, 214113.
- [48] Sun, Q. Libcint: an efficient general integral library for gaussian basis functions. *J. Comput. Chem.* **2015**, *36*, 1664–1671.
- [49] Lehtola, S.; Steigemann, C.; Oliveira, M. J. T.; Marques, M. A. L. Recent developments in LIBXC – a comprehensive library of functionals for density functional theory. *SoftwareX* **2018**, *7*, 1–5.
- [50] Marques, M. A. L.; Oliveira, M. J. T.; Burnus, T. LIBXC: a library of exchange and correlation functionals for density functional theory. *Comput. Phys. Commun.* **2012**, *183*, 2272–2281.
- [51] Hermes, M. R. MRH. GitHub, 2024; <https://github.com/MatthewRHermes/mrh>.
- [52] PYSCF-FORGE. GitHub, 2024; <https://github.com/pyscf/pyscf-forge>.
- [53] Wang, L.-P.; Song, C. Geometry optimization made simple with translation and rotation coordinates. *J. Chem. Phys.* **2016**, *144*, 214108.
- [54] Perdew, J. P.; Burke, K.; Ernzerhof, M. Generalized gradient approximation made simple. *Phys. Rev. Lett.* **1996**, *77*, 3865–3868.
- [55] Li Manni, G. et al. The OpenMolcas web: A community-driven approach to advancing computational chemistry. *J. Chem. Theory Comput.* **2023**, *19*, 6933–6991.
- [56] Ghigo, G.; Roos, B. O.; Malmqvist, P.-Å. A modified definition of the zeroth-order Hamiltonian in multiconfigurational perturbation theory (CASPT2). *Chem. Phys. Lett.* **2004**, *396*, 142–149.
- [57] Forsberg, N.; Malmqvist, P.-Å. Multiconfiguration perturbation theory with imaginary level shift. *Chem. Phys. Lett.* **1997**, *274*, 196–204.
- [58] Nishimoto, Y.; Battaglia, S.; Lindh, R. Analytic first-order derivatives of (XMS, XDW, and RMS variants of the CASPT2 and RASPT2 methods. *J. Chem. Theory Comput.* **2022**, *18*, 4269–4281.

- [59] Hariharan, P. C.; Pople, J. A. The influence of polarization functions on molecular orbital hydrogenation energies. *Theoretica chimica acta* **1973**, *28*, 213–222.
- [60] Knowles, P. J.; Werner, H.-J. Internally contracted multiconfiguration-reference configuration interaction calculations for excited states. *Theor. Chim. Acta* **1992**, *84*, 95–103.
- [61] Werner, H.-J.; Knowles, P. J. An efficient internally contracted multiconfiguration-reference configuration interaction method. *J. Chem. Phys.* **1988**, *89*, 5803–5814.
- [62] Knowles, P. J.; Werner, H.-J. An efficient method for the evaluation of coupling coefficients in configuration interaction calculations. *Chem. Phys. Lett.* **1988**, *145*, 514–522.
- [63] Koch, H.; Christiansen, O.; Jørgensen, P.; Sanchez de Merás, A. M.; Helgaker, T. The CC3 model: An iterative coupled cluster approach including connected triples. *J. Chem. Phys.* **1997**, *106*, 1808–1818.
- [64] Hutton, R. F.; Steel, C. Photoisomerization of azomethane. *J. Am. Chem. Soc.* **1964**, *86*, 745–746.
- [65] Robin, M. B.; Hart, R. R.; Kuebler, N. A. Electronic states of the azoalkanes. *J. Am. Chem. Soc.* **1967**, *89*, 1564–1572.
- [66] Liu, R.; Cui, Q.; Dunn, K. M.; Morokuma, K. Ab initio molecular orbital study of the mechanism of photodissociation of trans-azomethane. *J. Chem. Phys.* **1996**, *105*, 2333–2345.
- [67] Szalay, P. G.; Aquino, A. J. A.; Barbatti, M.; Lischka, H. Theoretical study of the excitation spectrum of azomethane. *Chem. Phys.* **2011**, *380*, 9–16.
- [68] Barbatti, M. Velocity adjustment in surface hopping: ethylene as a case study of the maximum error caused by direction choice. *J. Chem. Theory Comput.* **2021**, *17*, 3010–3018.
- [69] Diau, E. W.-G.; Abou-Zied, O. K.; Scala, A. A.; Zewail, A. H. Femtosecond Dynamics of Transition States and the Concept of Concertedness: Nitrogen Extrusion of Azomethane Reactions. *J. Am. Chem. Soc.* **1998**, *120*, 3245–3246.
- [70] Diau, E. W.-G.; Zewail, A. H. Femtochemistry of trans-Azomethane: A Combined Experimental and Theoretical Study. *ChemPhysChem* **2003**, *4*, 445–456.
- [71] North, S. W.; Longfellow, C. A.; Lee, Y. T. The near ultraviolet photodissociation dynamics of azomethane. *J. Chem. Phys.* **1993**, *99*, 4423–4429.
- [72] Bracker, A. S.; North, S. W.; Suits, A. G.; Lee, Y. T. The near ultraviolet dissociation dynamics of azomethane: Correlated V-T energy disposal and product appearance times. *J. Chem. Phys.* **1998**, *109*, 7238–7245.
- [73] Scott, T. R.; Oakley, M. S.; Hermes, M. R.; Sand, A. M.; Lindh, R.; Truhlar, D. G.; Gagliardi, L. Analytic gradients for multiconfiguration pair-density functional theory with density fitting: development and application to geometry optimization in the ground and excited states. *J. Chem. Phys.* **2021**, *154*, 074108.

TOC GRAPHIC



Supporting Information: Semiclassical Nonadiabatic Molecular Dynamics Using Linearized Pair-Density Functional Theory

Matthew R. Hennefarth,¹ Donald G. Truhlar,^{2,*} and Laura Gagliardi^{3,4,†}

¹*Department of Chemistry and Chicago Center for Theoretical Chemistry, University of Chicago, Chicago, IL 60637, USA*

²*Department of Chemistry, Chemical Theory Center, and Minnesota Supercomputing Institute, University of Minnesota, Minneapolis, MN 55455-0431, USA*

³*Department of Chemistry, Pritzker School of Molecular Engineering, The James Franck Institute, and Chicago Center for Theoretical Chemistry, University of Chicago, Chicago, IL 60637, USA*

⁴*Argonne National Laboratory, 9700 S. Cass Avenue, Lemont, IL 60439, USA*

(Dated: September 13, 2024)

CONTENTS

SI. Supplemental Figures	S2
SII. Optimized Geometries	S5
A. <i>cis</i> -azomethane	S5
B. <i>trans</i> -azomethane	S7
SIII. Wigner Distribution Frequencies	S8
SIV. Example Input Files	S9
A. SHARC Input Files	S9
B. PySCF Template Files	S9

* corresponding author: truhlar@umn.edu

† corresponding author: lgagliardi@uchicago.edu

SI. SUPPLEMENTAL FIGURES

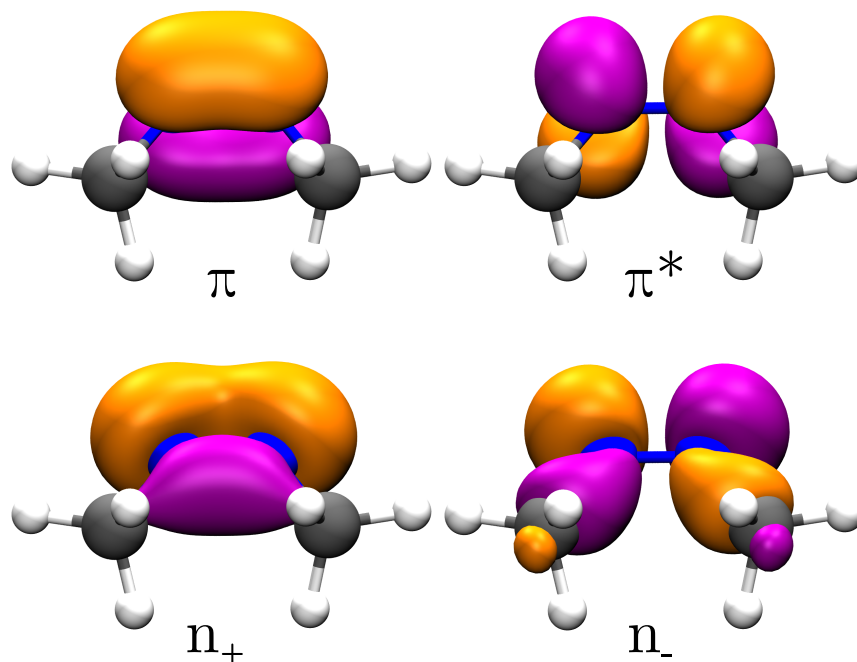


FIG. S1. Smaller (6,4) active space natural orbitals used for the *cis*-azomethane calculations consisting of the N–N π, π^* orbitals and the symmetric (n^+) and antisymmetric (n^-) nitrogen lone pair orbitals. The geometry is optimized at the L(2)-tPBE(6,4)/6-31G* level of theory. Isosurface value of 0.06.

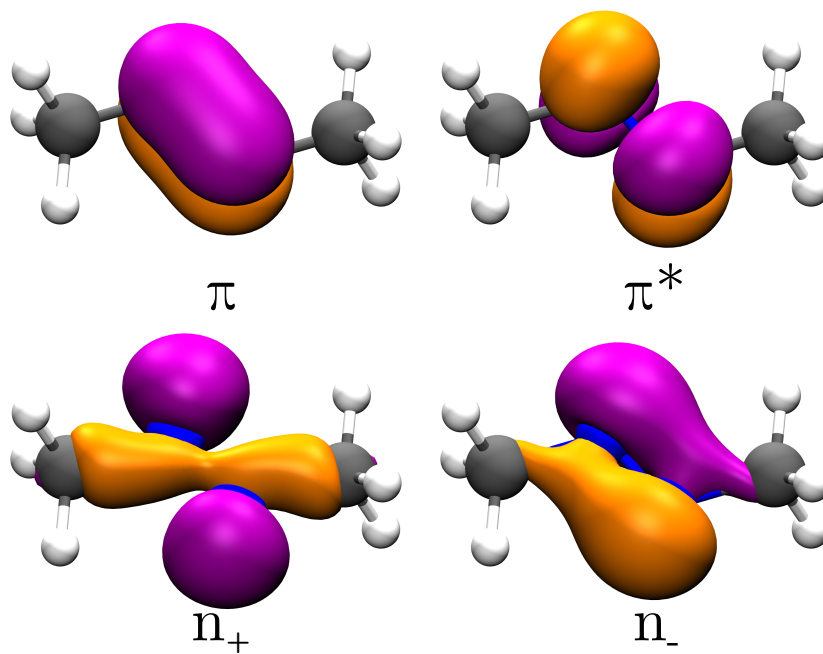


FIG. S2. Smaller (6,4) active space natural orbitals used for the *trans*-azomethane calculations consisting of the N–N π, π^* orbitals and the symmetric (n^+) and antisymmetric (n^-) nitrogen lone pair orbitals. The geometry is optimized at the L(2)-tPBE(6,4)/6-31G* level of theory. Isosurface value of 0.06.

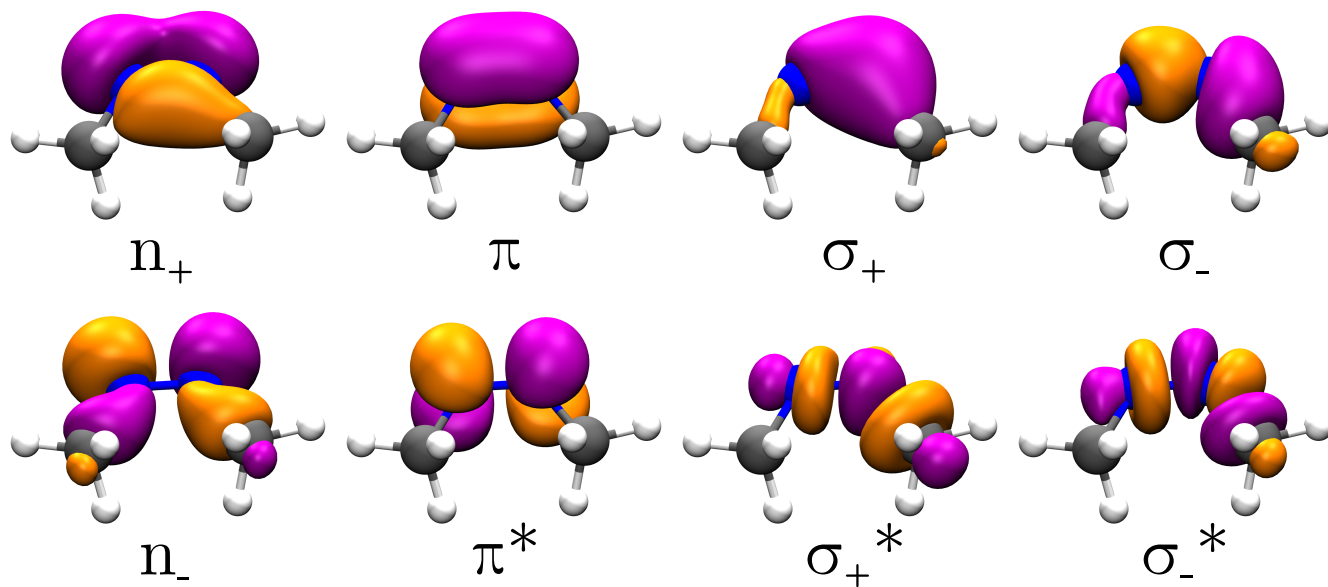


FIG. S3. Larger (10, 8) active space natural orbitals used for the *cis*-azomethane calculations consisting of the N–N π, π^* orbitals, the symmetric (n^+) and antisymmetric (n^-) nitrogen lone pair orbitals, and symmetric (σ_+, σ_+^*) and antisymmetric (σ_-, σ_-^*) N–N and N–C bonding and anti-bonding orbitals. The geometry is optimized at the L(2)-tPBE(10,8)/6-31G* level of theory. Isosurface value of 0.06.

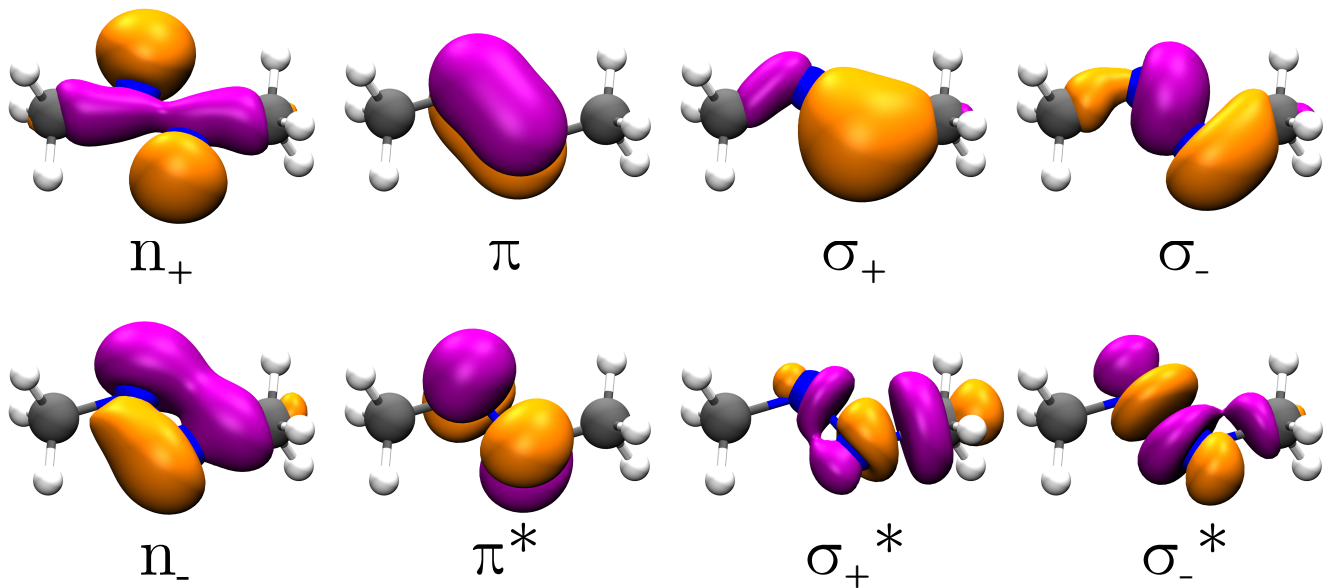


FIG. S4. Larger (10, 8) active space natural orbitals used for the *trans*-azomethane calculations consisting of the N–N π, π^* orbitals, the symmetric (n^+) and antisymmetric (n^-) nitrogen lone pair orbitals, and symmetric (σ_+, σ_+^*) and antisymmetric (σ_-, σ_-^*) N–N and N–C bonding and anti-bonding orbitals. The geometry is optimized at the L(2)-tPBE(10,8)/6-31G* level of theory. Isosurface value of 0.06.

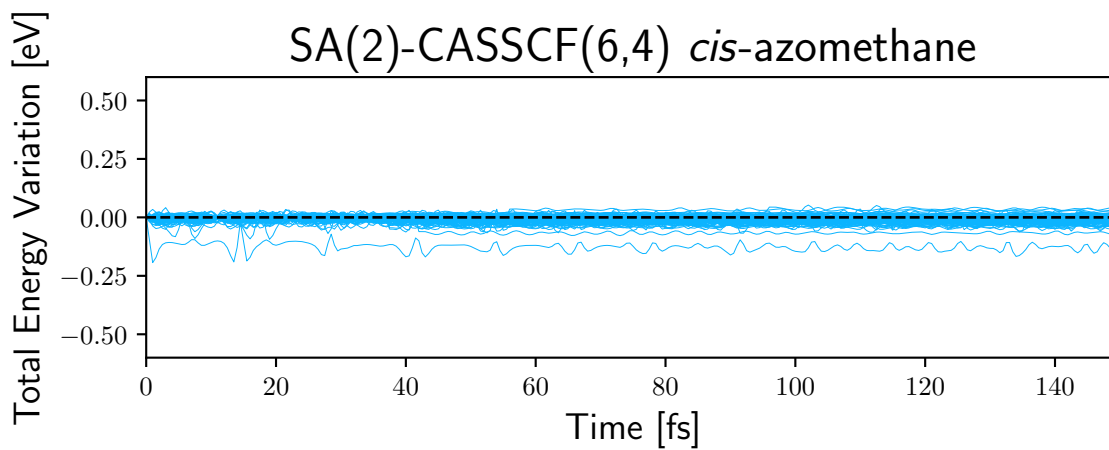


FIG. S5. Total energy variation as functions of time for SA(2)-CASSCF(6,4) starting in the *cis* isomer.

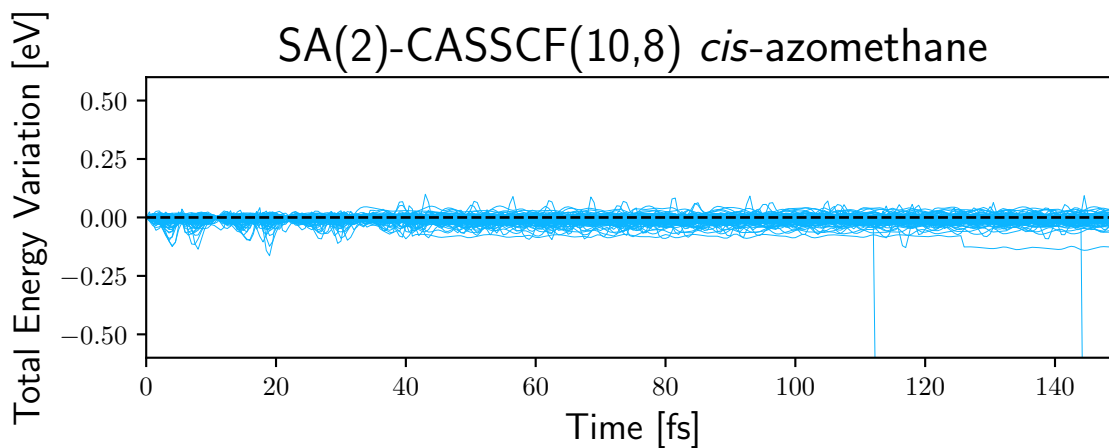


FIG. S6. Total energy variation as functions of time for SA(2)-CASSCF(10,8) starting in the *cis* isomer.

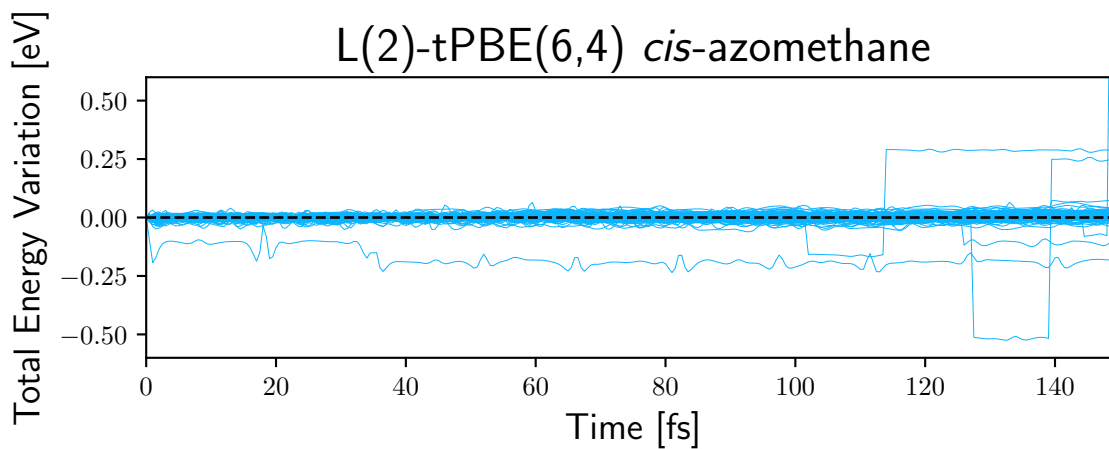


FIG. S7. Total energy variation as functions of time for L(2)-tPBE(6,4) starting in the *cis* isomer.

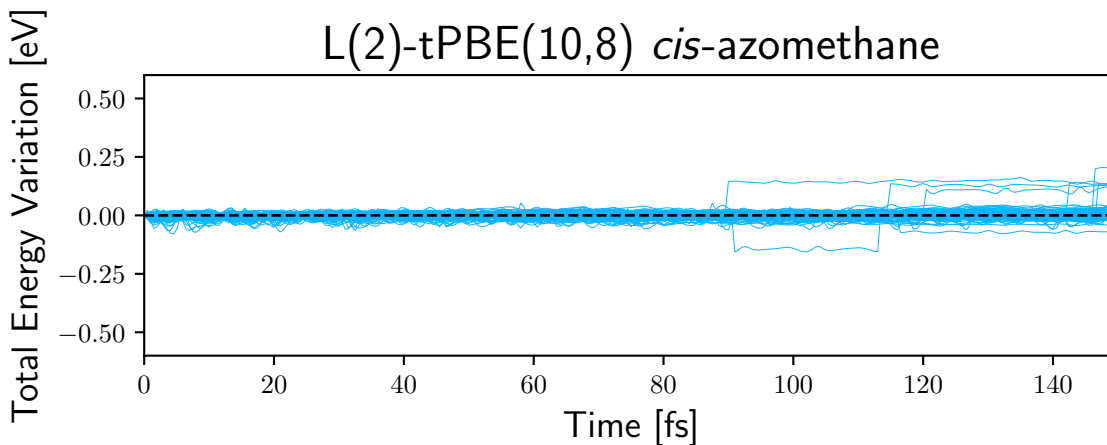


FIG. S8. Total energy variation as functions of time for L(2)-tPBE(10,8) starting in the *cis* isomer.

SII. OPTIMIZED GEOMETRIES

A. *cis*-azomethane

TABLE S1. SA(2)-CASSCF(6,4)/6-31G* *cis*-azomethane equilibrium ground state geometry (in Å). State 0 energy: $-188.083\,576\,391\,55$ hartrees. State 1 energy: $-187.950\,097\,843\,184$ hartrees

N	0.10301	-0.00000	-0.02243
N	0.10302	0.00000	1.22244
C	1.36738	-0.00000	1.95857
C	1.36737	0.00000	-0.75857
H	1.12869	-0.00000	-1.81190
H	1.95786	0.88156	-0.53395
H	1.95786	-0.88156	-0.53395
H	1.12870	0.00000	3.01190
H	1.95787	-0.88156	1.73395
H	1.95787	0.88156	1.73395

TABLE S2. SA(2)-CASSCF(10,8)/6-31G* *trans*-azomethane equilibrium ground state geometry (in Å). State 0 energy: $-188.151\,684\,469\,685$ hartrees. State 1 energy: $-188.010\,337\,616\,342$ hartrees

N	0.07074	-0.00000	-0.01687
N	0.09137	-0.00000	1.24884
C	1.36379	0.00000	1.96564
C	1.38946	-0.00000	-0.77415
H	1.13468	-0.00000	-1.82306
H	1.96992	0.88500	-0.54378
H	1.96992	-0.88501	-0.54378
H	1.14078	0.00000	3.02257
H	1.94948	-0.88187	1.73231
H	1.94948	0.88187	1.73231

TABLE S3. L(2)-tPBE(6,4)/6-31G* *cis*-azomethane equilibrium ground state geometry (in Å). State 0 energy: -188.981 625 763 722 hartrees. State 1 energy: -188.860 488 885 797 hartrees

N	0.07770	0.00000	-0.02126
N	0.07770	-0.00000	1.22126
C	1.36730	0.00000	1.96012
C	1.36730	-0.00000	-0.76013
H	1.13090	0.00000	-1.83272
H	1.96945	0.89576	-0.52359
H	1.96945	-0.89576	-0.52359
H	1.13090	-0.00000	3.03271
H	1.96945	-0.89576	1.72358
H	1.96945	0.89576	1.72358

TABLE S4. L(2)-tPBE(10,8)/6-31G* *cis*-azomethane equilibrium ground state geometry (in Å). State 0 energy: -188.972 556 382 39 hartrees. State 1 energy: -188.851 010 312 274 hartrees

N	0.07872	0.00000	-0.02725
N	0.07846	-0.00000	1.22145
C	1.36691	0.00000	1.96144
C	1.36558	-0.00000	-0.76078
H	1.13437	0.00000	-1.83453
H	1.96817	0.89509	-0.52342
H	1.96817	-0.89509	-0.52342
H	1.12979	-0.00000	3.03391
H	1.96971	-0.89577	1.72628
H	1.96971	0.89577	1.72628

TABLE S5. XMS(2)-CASPT2(6,4)/6-31G* *cis*-azomethane equilibrium ground state geometry (in Å). State 0 energy: -188.641 652 34 hartrees. State 1 energy: -188.517 342 93 hartrees

N	0.08101	-0.00000	-0.02854
N	0.08102	0.00000	1.22853
C	1.37150	-0.00000	1.95678
C	1.37150	0.00000	-0.75679
H	1.13692	-0.00000	-1.82053
H	1.96267	0.89026	-0.51646
H	1.96267	-0.89026	-0.51646
H	1.13692	0.00000	3.02052
H	1.96267	-0.89026	1.71645
H	1.96267	0.89026	1.71645

TABLE S6. XMS(2)-CASPT2(10,8)/6-31G* *cis*-azomethane equilibrium ground state geometry (in Å). State 0 energy: -188.642 361 68 hartrees. State 1 energy: -188.514 899 81 hartrees

N	0.07662636	-0.00000058	-0.02808695
N	0.08123588	0.00000056	1.23096375
C	1.37101405	-0.00000013	1.95816387
C	1.37358989	0.00000015	-0.75946656
H	1.13807799	-0.00000009	-1.82268836
H	1.96346666	0.89019838	-0.51909243
H	1.96346693	-0.89019787	-0.51909223
H	1.13772167	0.00000008	3.02223585
H	1.96220512	-0.89029263	1.71850668
H	1.96220543	0.89029212	1.71850640

B. *trans*-azomethaneTABLE S7. SA(2)-CASSCF(6,4)/6-31G* *trans*-azomethane equilibrium ground state geometry (in Å). State 0 energy: -188.103 159 734 455 hartrees. State 1 energy: -187.963 485 191 687 hartrees

C	1.42953	-0.00007	1.67795
N	0.05054	-0.00036	1.21666
N	-0.04952	0.00221	-0.01951
C	-1.42851	0.00182	-0.48081
H	-2.13503	-0.00070	0.34027
H	-1.57510	-0.87250	-1.10414
H	-1.57675	0.87865	-1.10017
H	2.13605	0.00249	0.85687
H	1.57786	-0.87688	2.29736
H	1.57603	0.87428	2.30124

TABLE S8. SA(2)-CASSCF(10,8)/6-31G* *trans*-azomethane equilibrium ground state geometry (in Å). State 0 energy: -188.170 501 871 954 hartrees. State 1 energy: -188.024 022 048 082 hartrees

C	1.45314	-0.00007	1.69160
N	0.02402	-0.00045	1.23536
N	-0.05818	0.00224	-0.02640
C	-1.43702	0.00185	-0.49026
H	-2.14743	-0.00071	0.32701
H	-1.58171	-0.87246	-1.11389
H	-1.58348	0.87866	-1.10994
H	2.14130	0.00246	0.85704
H	1.59811	-0.88018	2.30565
H	1.59636	0.87760	2.30954

TABLE S9. L(2)-tPBE(6,4)/6-31G* *trans*-azomethane equilibrium ground state geometry (in Å). State 0 energy: -188.996 344 537 52 hartrees. State 1 energy: -188.865 879 862 179 hartrees

C	1.43882	0.00006	1.67998
N	0.04077	-0.00162	1.21943
N	-0.03974	0.00091	-0.02229
C	-1.43780	0.00190	-0.48283
H	-2.15752	0.00003	0.35275
H	-1.58278	-0.88537	-1.12157
H	-1.58291	0.89195	-1.11768
H	2.15854	0.00338	0.84440
H	1.58555	-0.88981	2.31469
H	1.58218	0.88750	2.31885

TABLE S10. L(2)-tPBE(10,8)/6-31G* *trans*-azomethane equilibrium ground state geometry (in Å). State 0 energy: -188.986 328 119 442 hartrees. State 1 energy: -188.856 908 724 63 hartrees

C	1.44642	-0.00045	1.67018
N	0.04836	-0.00026	1.22108
N	-0.04490	0.00387	-0.02470
C	-1.44689	0.00212	-0.47350
H	-2.15885	-0.00118	0.36867
H	-1.59699	-0.88549	-1.11060
H	-1.60034	0.89193	-1.10650
H	2.16068	0.00189	0.82986
H	1.59943	-0.89004	2.30373
H	1.59821	0.88650	2.30750

TABLE S11. XMS(2)-CASPT2(6,4)/6-31G* *trans*-azomethane equilibrium ground state geometry (in Å). State 0 energy: -188.657 566 16 hartrees. State 1 energy: -188.525 008 82 hartrees

C	1.43442	-0.00004	1.68125
N	0.03796	-0.00042	1.22666
N	-0.03694	0.00222	-0.02951
C	-1.43340	0.00182	-0.48410
H	-2.13676	-0.00079	0.35317
H	-1.57729	-0.88082	-1.11323
H	-1.57910	0.88702	-1.10921
H	2.13778	0.00249	0.84397
H	1.58009	-0.88520	2.30642
H	1.57834	0.88264	2.31031

TABLE S12. XMS(2)-CASPT2(10,8)/6-31G* *trans*-azomethane equilibrium ground state geometry (in Å). State 0 energy: -188.657 124 85 hartrees. State 1 energy: -188.521 996 85 hartrees

C	1.43734	-0.00000	1.68324
N	0.03468	-0.00086	1.22847
N	-0.03867	0.00182	-0.02814
C	-1.43449	0.00187	-0.48550
H	-2.13979	-0.00054	0.35012
H	-1.57828	-0.88068	-1.11458
H	-1.57960	0.88701	-1.11062
H	2.13814	0.00272	0.84457
H	1.58402	-0.88533	2.30712
H	1.58175	0.88291	2.31104

III. WIGNER DISTRIBUTION FREQUENCIES

TABLE S13. Harmonic frequencies (in cm^{-1}) used to generate the Wigner distribution. All values are calculated at the SA(2)-CASSCF/6-31G* level of theory.

Mode	(6e,4o)	(10e,8o)
1	38.93	23.83
2	219.43	218.74
3	394.43	382.38
4	483.23	462.43
5	674.51	633.82
6	988.19	868.79
7	1079.67	1046.01
8	1109.45	1060.56
9	1207.55	1181.23
10	1218.56	1187.10
11	1310.13	1283.49
12	1563.25	1529.18
13	1581.86	1575.65
14	1619.49	1592.23
15	1629.09	1614.31
16	1643.78	1638.29
17	1666.49	1646.03
18	1741.98	1663.33
19	3213.77	3219.90
20	3220.45	3228.68
21	3282.26	3290.78
22	3286.79	3304.68
23	3322.10	3322.31
24	3324.46	3335.16

SIV. EXAMPLE INPUT FILES

A. SHARC Input Files

Example SHARC input file for trajectory surface hopping dynamics of *trans*-azomethane out to 400 fs with a nuclear time step of 0.5 fs.

```
printlevel 2

geomfile "geom"
veloc external
velocfile "veloc"

nstates 2
actstates 2
state 2 mch
coeff auto
rngseed 12118

ezero -188.0849123900
tmax 400.000000
stepsize 0.500000
nsubsteps 200
integrator fvv

method tsh
surf mch
coupling ktdc
nogradcorrect
ekinincorrect parallel_vel
reflect_frustrated none
decoherence_scheme edc
decoherence_param 0.1
hopping_procedure sharc
grad_all
select_directly
nospinorbit
output_format ascii
output_dat_steps 1
nophases_from_interface
ktdc_method gradient
```

B. PySCF Template Files

Example PYSCF.template file to perform L(2)-tPBE(6,4) with the 6-31G* basis set.

```
basis 6-31g*
ncas 4
nelecas 6
roots 2

method l-pdft
pdft-functional tpbe
grids-level 4
conv-tol 1e-7
conv-tol-grad 1e-4

max-cycle-macro 10000
grad-max-cycle 1000

verbose 3
```

Example PYSCF.template file to perform SA(2)-CASSCF(6,4) with the 6-31G* basis set.

```
basis 6-31g*
ncas 4
nelecas 6
```

```
roots 2

method casscf
conv-tol 1e-7
conv-tol-grad 1e-4

max-cycle-macro 10000
grad-max-cycle 1000

verbose 3
```